AIAA SciTech Forum
7-11 January 2019, San Diego, California
AIAA Scitech 2019 Forum

10.2514/6.2019-2143

Compressible Flamelet Model with Thickened Flame Closure in an All-Speed Combustion Solver

Siddharth Thakur* and Jeffrey Wright
Streamline Numerics, Inc., Gainesville, FL, 32609, U.S.A.
Matthias Ihme†
Stanford University

A robust unsteady turbulent compressible combustion modeling capability developed in a CFD solver called Loci-STREAM is presented in this paper. It utilizes the flamelet methodology extended to account for compressibility involving both ideal and real fluids. The ideal-gas thermodynamics is modeled by linearizing the specific heat ratio whereas the parameters needed for the cubic Peng Robinson equation of state are pre-tabulated for the evaluation of departure functions and a quadratic expression is used to model the attraction parameter. This compressible model is able to account for temperature and pressure variations from the baseline flamelet table. This solver integrates proven numerical methods for generalized grids and state-of-the-art physical models in a rule-based programming framework called Loci which allows: (a) seamless integration of multidisciplinary physics in a unified manner, and (b) automatic handling of parallel computing. The objective is to be able to routinely simulate unsteady combustion in complex geometries such as liquid rocket engines requiring large unstructured grids and complex multidisciplinary physics.

Downloaded by STANFORD UNIVERSITY on January 17, 2019 | http://arc.aiaa.org | DOI: 10.2514/6.2019-2143

I. Introduction

The use of high-fidelity analysis and design tools such as CFD early in the product development cycle of rocket engines is increasingly becoming more common as one way to alleviate testing costs and to develop these devices better, faster and cheaper. In the design of advanced propulsion systems, CFD plays a major role in defining the required performance over the entire flight regime, as well as in testing the sensitivity of the design to the different modes of operation. Thus, increased emphasis is being placed on developing and applying CFD models to simulate the flow field environments and performance of advanced propulsion systems. This necessitates the development of next generation computational tools which can be used effectively and reliably in a design environment by non-CFD specialists. The goal of the present work is to develop a computational tool capable of unsteady turbulent combustion using state-of-the-art flamelet methodology. Previous work has led to the development of a flamelet-based methodology for unsteady turbulent combustion in an all-speed pressure-based algorithm implemented in a rule-based framework [1]. The approach presented here extends this methodology to account for compressibility involving both ideal and real fluids. The basic ideas of this methodology were first presented by Ma et al. [2] within the framework of an explicit density-based finite volume solver. The ideal-gas thermodynamics is modeled by linearizing the specific heat ratio whereas the parameters needed for the cubic Peng Robinson equation of state are pre-tabulated for the evaluation of departure functions and a quadratic expression is used to model the attraction parameter. This compressible model is able to account for temperature and pressure variations from the baseline flamelet table using a computationally tractable pre-tabulated combustion chemistry in a thermodynamically consistent fashion.

The computational tool used as the basis for the present work is called Loci-STREAM [3]. It integrates proven numerical methods for generalized grids and state-of-the-art physical models in a novel rule-based programming framework called *Loci* [4] which allows: (a) seamless integration of multidisciplinary physics in a unified manner, and (b) automatic handling of massively parallel computing. An immediate application of interest is simulation of unsteady reacting flows in rocket combustion systems.

The framework for application development called *Loci* [4] is designed to reduce the complexity of assembling large-scale finite-volume applications as well as the integration of multiple applications in a multidisciplinary environment. Unlike traditional procedural programming systems (C, FORTRAN) in which one writes code with

* Senior Scientist, Streamline Numerics, Member AIAA.
† Associate Professor, Stanford University, Member AIAA.

Copyright © 2019 by Siddharth Thakur, Jeffrey Wright and Matthias Ihme. Published by the American Institute of Aeronautics and Astronautics, Inc., with permission.

subroutines, or object-oriented systems (C++, Java) in which objects are the major program components, *Loci* uses a rule-based framework for application design. Users of *Loci* write applications using a collection of "rules" and provide an implementation for each of the rules in the form of a C++ class. In addition, the user must create a database of "facts" which describe the particular knowns of the problem, such as boundary conditions. Once the rules and facts are provided, a query is made to have the system construct a solution. One of the interesting features of *Loci* is its ability to automatically determine the scheduling of events of the program to produce the answer to the desired query, as well as to test the consistency of the input to determine whether a solution is possible given the specified information. The other major advantage of *Loci* to the application developer is its automatic handling of domain decomposition and distribution of the problem to multiple processors

II. Flamelet Models

Accounting for the coupling between turbulence and the chemical reactions is one of the main difficulties in turbulent combustion modeling. An attractive approach (which forms the basis of flamelet modeling) in terms of computational cost is to reduce the dimensionality of the problem by utilizing the concept of conserved scalars [5]. The statistics of the conserved scalar is described with a presumed shape PDF. The problem is then transformed to the one of linking the conserved scalar to the reactive scalars such as species mass fractions and temperature. This step is often associated with assumptions regarding the flame structure and chemistry speed and/or complexity.

Conserved scalars are quantities that are unchanged by the chemical reactions. A normalized conserved scalar called the mixture fraction (Z) can then be defined such that it takes the value of 0 in the oxidizer stream and 1 in the fuel stream. Figure 1 shows the generic response of the heat release by a one-dimensional laminar diffusion flame in the form of the so-called S-shaped curve. The left plot in Figure 1 shows the heat release versus the Damkohler number whereas the right plot shows the corresponding variation of stoichiometric temperature with the stoichiometric scalar dissipation rate. Note that the stoichiometric scalar dissipation rate is related to the Damkohler number. The upper branch of the S-shaped curve represents the combusting regime. Starting from the upper branch, if the diffusion time scale is decreased (e.g. by increasing flow rates), the Da reduces and the heat generated by reactions are diffused from the reaction zone faster until reactions cannot keep up and the quenching limit is reached. After quenching, a regime of pure mixing without combustion, represented by the lower branch of the curve, is attained. Starting from the lower branch however, when the Da is increased the same path is not followed. Instead, the pure mixing regime exists until the ignition Da is reached. After ignition, a rapid transition to the upper branch follows. Referring to Figure 1, if the chemistry were assumed to be infinitely fast in the analysis of such a flame, flame stretching would not be captured. The infinitely fast chemistry approach corresponds to the dashed line in Figure 1. In this approach, the flame is completely described with the knowledge of mixing and hence the mixture fraction variable distribution.

On the other hand, if the flame is described by the mixture fraction variable and the scalar dissipation rate, finite-rate chemistry effects are recovered. However, whether the flame is extinct or ignited, corresponding to the lower or the

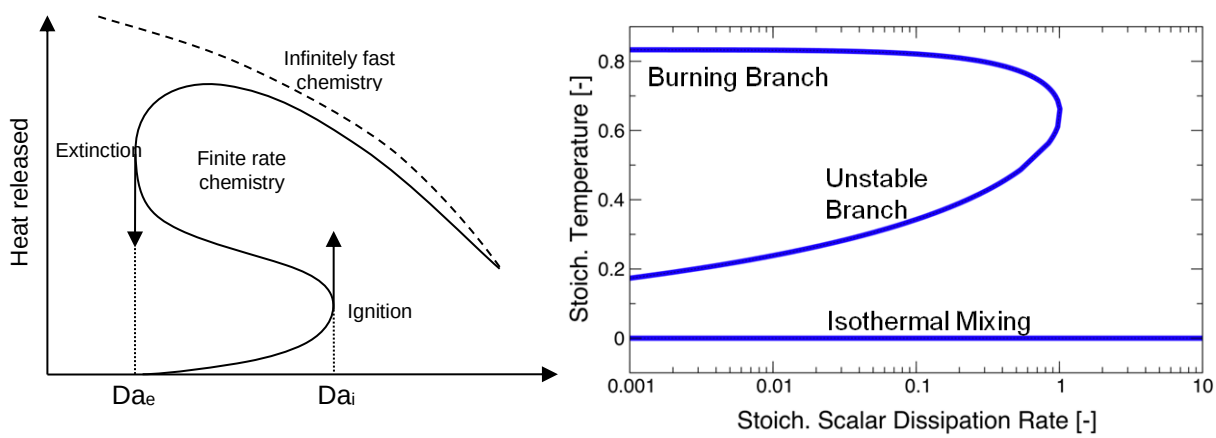

Figure 1. Generic response of the heat released by a 1-dimensional laminar diffusion flame.

Downloaded by STANFORD UNIVERSITY on January 17, 2019 | http://arc.aiaa.org | DOI: 10.2514/6.2019-2143

upper branches of the solid curve in Figure 1(left), depends on the path followed as discussed above. A third quantity is then needed to fully determine the regime. This quantity, called the progress variable, will be discussed later in the context of extensions to the basic flamelet model.

Flamelet models are based on the view of a turbulent diffusion flame as an ensemble of stretched laminar flamelets (see Figure 2). Inherent to this view is the assumption of a thin reaction zone which is thinner than the scale of a Kolmogorov eddy. The effect of turbulence is therefore limited to the deformation and stretching of the flame sheet but does not penetrate the reaction zone. Flamelets are then thin laminar reactive diffusive layers embedded in an otherwise non-reacting turbulent flow field. The local reactive-diffusive balance in flamelets are viewed as similar to that of a laminar flame with the same Z and χ.

Flamelet equations can be derived via a Crocco-type coordinate transformation of the species mass fraction and energy equations. The original coordinate system is selected such that the x_2 and x_3 are locally aligned to the flame surface which is determined by the stoichiometric mixture fraction, $Z = Z_{st}$. Then x_1, which is normal to the stoichiometric surface, is replaced by Z. The transformation, as illustrated in Figure 2, can be represented as:

$$(t, x_1, x_2, x_3) \rightarrow (\tau, Z, Z_1, Z_2) \tag{1}$$

where $\tau = t$, $Z = x_1$, $Z_2 = x_2$ and $Z_3 = x_3$. Thus, species and energy equations can be transformed in the mixture fraction space to yield:

$$\rho \frac{\partial Y_i}{\partial \tau} = \rho \frac{\chi}{2} \frac{\partial^2 Y_i}{\partial Z^2} + \dot{\omega}_i \tag{2}$$

$$\rho \frac{\partial T}{\partial \tau} = \rho \frac{\chi}{2} \frac{\partial^2 T}{\partial Z^2} - \sum_{i=1}^{n} \frac{h_i}{C_p} \dot{\omega}_i + \frac{1}{C_p} \frac{\partial p}{\partial \tau} \tag{3}$$

In Eqs. (7) and (8), the scalar dissipation rate appears as an external parameter. Pitsch et al. considered a semi-infinite mixing layer to obtain the following analytical expression:

$$\chi(Z) = \chi_{st} \frac{Z^2}{Z_{st}^2} \frac{\ln(Z)}{\ln(Z_{st})} \tag{4}$$

In space propulsion systems, fuel conversion and chemical reactions occur on time scales that are typically significantly shorter compared to the characteristic kinematic scales that are associated with the turbulence and hydrodynamics. In these large-Damkohler number flows, all thermochemical quantities are in steady state. As a consequence, transient effects in Eqs. (2) and (3) become negligible, so that the species and temperature distribution can accurately be presented by the solution of the steady flamelet equations. In this context, it is important to point out that, although transient effects in the flamelet equations are neglected, the dynamics of the combustion processes

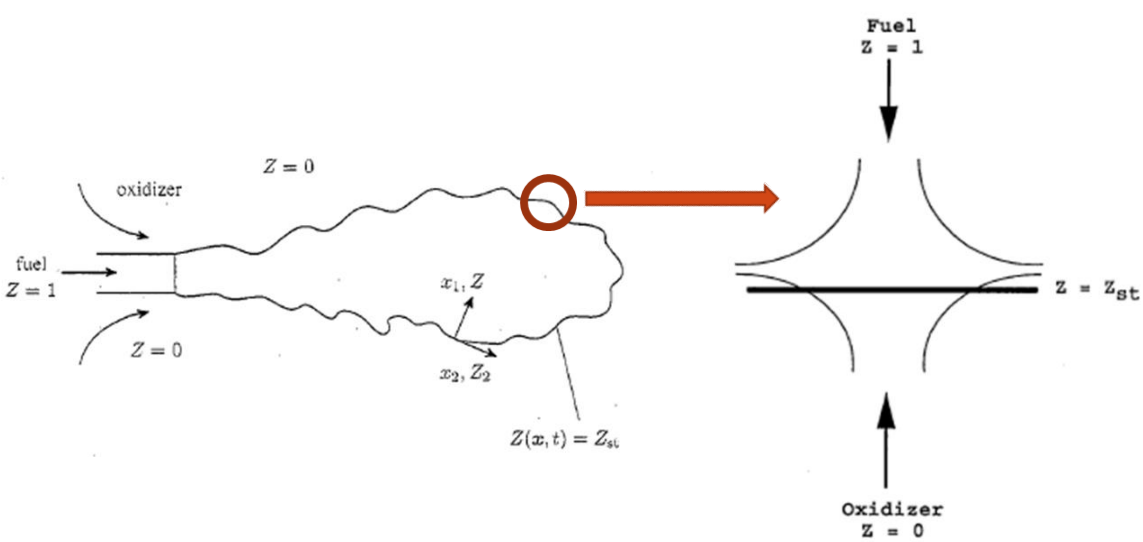

Figure 2. Flamelet model concept.

Downloaded by STANFORD UNIVERSITY on January 17, 2019 | http://arc.aiaa.org | DOI: 10.2514/6.2019-2143

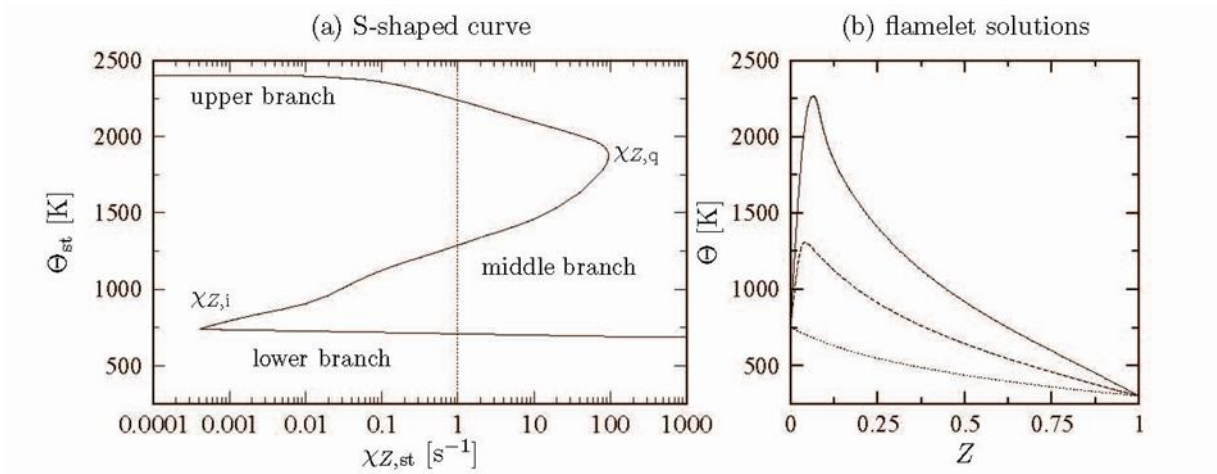

Figure 3. The S-shaped curve illustrating multiple solutions resulting from steady flamelet model (SFM).

and the interaction between turbulence and reaction chemistry is fully accounted for; the only limitation that arises from the steady flamelet model is that chemical effects that evolve on relatively slower temporal scales compared to the characteristic hydrodynamics scales (such as during auto-ignition or slow nitric-oxide pollutant formation), are not accurately represented with the steady flamelet model.

With Eq.(4), the flamelet equations (Eqs. (2) and (3)) can be parameterized by only χ_{st}. Then the solution to those equations takes the functional form:

$$Y_i, T = f(Z, \chi_{st}) \tag{5}$$

Using a specified reaction mechanism, Eq. (5) can be tabulated into a library (table) as a preprocessing step for turbulent combustion computations.
To obtain the mean properties, the flamelet results are convoluted with a joint PDF, as follows:

$$\widetilde{Y_i} = \int_Z \int_\chi Y_i P(Z, \chi) \mathrm{d}\chi \mathrm{d}Z \tag{6}$$

Assuming that the mixture fraction and the scalar dissipation are uncorrelated, we have

$$\widetilde{Y_i} = \int_Z \int_\chi Y_i P(Z) P(\chi) \mathrm{d}\chi \mathrm{d}Z \tag{7}$$

The PDFs are constructed so as to reproduce $\tilde{Z}, \widetilde{Z''^2}$ and $\tilde{\chi}$. As a result, the mean composition of the mixture can be obtained with the knowledge of these three quantities. Flamelet equations can be pre-solved for a number of Z and χ values and the results can be integrated through the PDF's constructed for a range of $\tilde{Z}, \widetilde{Z''^2}$ and $\tilde{\chi}$ values, enabling a tabulation which can be represented as

$$\tilde{Z}, \widetilde{Z''^2}, \tilde{\chi} \xrightarrow{PDF\ table\ lookup} Y_i\ , T \tag{8}$$

This is referred to as the Steady Flamelet Model (SFM).

A major limitation of the steady flamelet model (SFM) arises from the parameterization of the thermochemical quantities, in which mixture fraction Z and scalar dissipation rate $\chi_{Z,st}$ are used. In particular, this parameterization of the entire flamelet solution space is not unique and results in multiple solutions for $\chi_{Z,i} \leq \chi_{Z,st} \leq \chi_{Z,q}$ where "i" represents auto-ignition and "q" represents flame quenching or extinction (see Figure 3a). This can be seen in Figure 3(b) which shows that three flamelet solutions (temperature profiles) are possible – corresponding to the three branches of the S-shaped curve – for the same scalar dissipation rate of $\chi_{Z,st}$=1 s^{-1} (given by the location of the dashed vertical line in Figure 3a). In the SFM approach, in order to obtain a unique solution, the upper (burning) branch is always picked, thus excluding any possibility of unsteady effects such as auto-ignition or local flame quenching. To overcome this limitation, a flamelet/progress variable (FPV) formulation has been developed ([6,7]). In this model, a reaction

Downloaded by STANFORD UNIVERSITY on January 17, 2019 | http://arc.aiaa.org | DOI: 10.2514/6.2019-2143

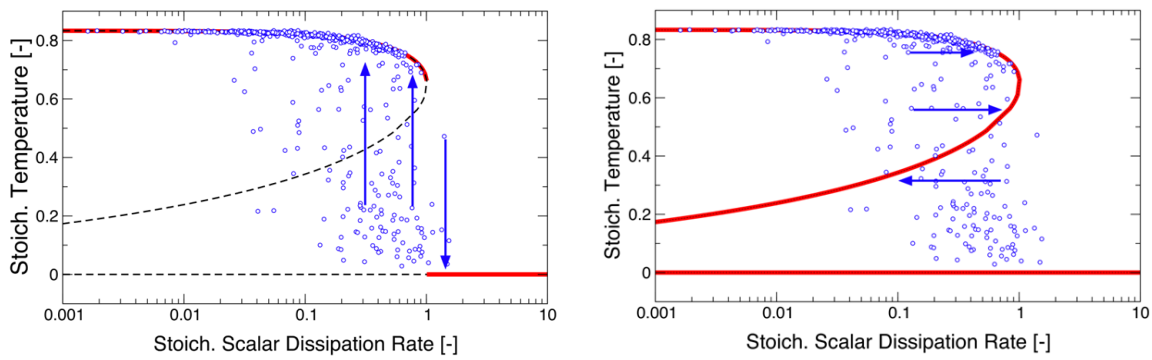

Figure 4. Comparison of the Steady Flamelet Model (SFM) and the Flamelet/Progress variable (FPV) model: the left plot shows the horizontal projection used in the SFM and the right plot shows the vertical projection used in the FPV model. The solid (red) lines show the accessible solution in the SFM (left) and the FPV (right) models.

progress variable C has been introduced as a parameter, which replaces the scalar dissipation rate. This model, has previously been implemented in Loci-STREAM [1,8]. The progress variable is defined using a linear combination of reaction product species, which allows a unique identification of each single flamelet along the entire S-shape curve. This effectively means that, compared to the SFM model, the FPV model employs a horizontal projection onto the S-shaped curve, as shown in Figure 4, so that a unique flamelet solution is always obtained along the S-shaped curve.

III. Compressible Flamelet Model

The Loci-STREAM flow solver [3] is based on the SIMPLE (Semi-Implicit Method for Pressure-Linked Equations) algorithm [9]. It uses a control volume approach with a collocated arrangement for the velocity components and the scalar variables like pressure. Pressure-velocity decoupling is prevented by employing the momentum interpolation approach [10]; this involves adding a fourth-order pressure dissipation term while estimating the mass flux at the control volume interfaces. The velocity components are computed from the respective momentum equations. The velocity and the pressure fields are corrected using a pressure correction (p') equation. The correction procedure leads to a continuity-satisfying velocity field. The whole process is repeated until the desired convergence is reached. Detached-Eddy Simulation (DES) [11] is employed for turbulent flow simulations. In this work, an extension to the flamelet model in Loci-STREAM [1] is developed to account for the pressure variations in rocket combustors.

The approach presented here utilizes the flamelet (FPV) methodology extended to account for compressibility involving both ideal and real fluids. The basic ideas of this methodology were first presented by Ma et al. [2]. The ideal-gas thermodynamics is modeled by linearizing the specific heat ratio whereas the parameters needed for the cubic Peng Robinson equation of state are pre-tabulated for the evaluation of departure functions and a quadratic expression is used to model the attraction parameter. This compressible model is able to account for temperature and pressure variations from the baseline flamelet table using a computationally tractable pre-tabulated combustion chemistry in a thermodynamically consistent fashion.

A. Governing Equations

Unlike the previous flamelet model in Loci-STREAM [1] which was designed primarily to handle low-Mach number flow situations (as found in the combustor section) the new compressible capability presented here seamlessly handles all parts of the combustion domain, including the upstream fuel and oxidizer manifold sections, the combustion chamber and the highly-compressible nozzle. The governing equations used in this approach are the Favre-averaged Navier-Stokes equations, in addition to the transport equations for flamelet manifold variables Z and C, as given below:

$$\frac{\partial \bar{\rho}}{\partial t} + \frac{\partial \bar{\rho} u_j}{\partial x_j} = 0 \tag{9}$$

Downloaded by STANFORD UNIVERSITY on January 17, 2019 | http://arc.aiaa.org | DOI: 10.2514/6.2019-2143

$$\frac{\partial \bar{\rho} u_i}{\partial t} + \frac{\partial \bar{\rho} u_j u_i}{\partial x_j} = -\frac{\partial \bar{p}}{\partial x_i} + \frac{\partial}{\partial x_j}\left(\tilde{\tau}_{ij} - \overline{\rho u_i'' u_j''}\right) \tag{10}$$

$$\begin{aligned}\frac{\partial \bar{\rho} E}{\partial t} + \frac{\partial}{\partial x_j}\left(\bar{\rho} u_j E\right) &= \frac{\partial}{\partial x_j}\left[\left(\frac{\lambda}{c_p} + \frac{\mu_t}{Pr_t}\right)\frac{\partial h}{\partial x_j}\right] + \frac{\partial}{\partial x_j}\left(\sum_{k=1}^{NS}\left(\bar{\rho} D_k - \frac{\lambda}{c_p}\right) h_k \frac{\partial Y_k}{\partial x_j}\right) + \\ &\frac{\partial}{\partial x_j}\left[u_j\left(\tilde{\tau}_{ij} - \overline{\rho u_i'' u_j''}\right) - u_j p\right]\end{aligned} \tag{11}$$

$$\frac{\partial \bar{\rho} Z}{\partial t} + \frac{\partial \bar{\rho} u_j Z}{\partial x_j} = \frac{\partial}{\partial x_j}\left[\left(\bar{\rho} D + \frac{\mu_t}{Sc_t}\right)\frac{\partial Z}{\partial x_j}\right] \tag{12}$$

$$\frac{\partial \bar{\rho} Z''^2}{\partial t} + \frac{\partial \bar{\rho} u_j Z''^2}{\partial x_j} = \frac{\partial}{\partial x_j}\left(\frac{\mu_t}{Sc_t}\frac{\partial Z''^2}{\partial x_j}\right) + 2\frac{\mu_t}{Sc_t}\frac{\partial Z}{\partial x_j}\frac{\partial Z}{\partial x_j} - \bar{\rho}\chi \tag{13}$$

$$\frac{\partial \rho C}{\partial t} + \frac{\partial \rho u_j C}{\partial x_j} = \frac{\partial}{\partial x_j}\left(\rho \alpha \frac{\partial C}{\partial x_j}\right) + \rho \dot{\omega}_C \tag{14}$$

where

$$\begin{aligned}\tilde{\tau}_{ij} &= \mu\left(\frac{\partial u_i}{\partial x_j} + \frac{\partial u_j}{\partial x_i}\right) - \frac{2}{3}\mu\frac{\partial u_k}{\partial x_k}\delta_{ij} \\ -\overline{\rho u_i'' u_j''} &= \mu_t\left(\frac{\partial u_i}{\partial x_j} + \frac{\partial u_j}{\partial x_i}\right) - \frac{2}{3}\mu_t\frac{\partial u_k}{\partial x_k}\delta_{ij} - \frac{2}{3}\bar{\rho} k \delta_{ij}\end{aligned} \tag{15}$$

$$\chi(Z) = c_\chi c_\mu \omega Z''^2, \qquad where \;\; c_\chi = 2,\; c_\mu = 0.09 \tag{16}$$

For DES/LES, Eq. (13) is replaced by:

$$Z''^2 = C_s \Delta^2 \left|\nabla \tilde{Z}\right|^2 \tag{17}$$

All thermochemical quantities are parameterized in terms of mixture fraction *Z* and progress variable *C*, and the turbulence/chemistry interaction is modeled through a presumed PDF closure model. The parameterization can be represented as:

$$\tilde{Z}, \tilde{Z}''^2, \tilde{C} \xrightarrow{\;flamelet\ lookup\ table\;} \tilde{Y}_i \tag{18}$$

B. Thermodynamics and Transport Properties

Augmenting the above governing PDEs is a flamelet tabulation, based on the Peng-Robinson equation of state (PR-EoS) that provides both ideal-gas reference state and real-fluid thermodynamic information about the mixture (for a given Z and C) so that the density and temperature of the fluid may be recovered from the solved state variables (p, E, Z and C) using an efficient bracketed secant method iterative process. The Peng-Robinson (PR) equation of state [12] is employed for the evaluation of thermodynamic quantities; it can be written as:

$$p = \frac{RT}{v-b} - \frac{a}{v^2 + 2bv - b^2} \tag{19}$$

where p is the pressure, R is the gas constant, T is the temperature, v is the specific volume, and the attraction parameter *a* and effective molecular volume *b* are dependent on temperature and composition to account for effects of intermolecular forces. For mixtures, the parameters *a* and *b* are evaluated as

$$a = \sum_{\alpha=1}^{N_s}\sum_{\beta=1}^{N_s} X_\alpha X_\beta a_{\alpha\beta} \tag{20}$$

$$b = \sum_{\alpha=1}^{N_s} X_\alpha b_\alpha \tag{21}$$

where X_α is the mole fraction of species α. Extended corresponding states principle and single-fluid assumption for mixtures are adopted [13,14]. The parameters *a* and *b* are evaluated using the recommended mixing rules by Harstad et al. [15].

Downloaded by STANFORD UNIVERSITY on January 17, 2019 | http://arc.aiaa.org | DOI: 10.2514/6.2019-2143

$$a_{\alpha\beta} = 0.457236 \frac{\left(RT_{c,\alpha\beta}\right)^2}{p_{c,\alpha\beta}} \left(1 + c_{\alpha\beta}\left(1 - \sqrt{\frac{T}{T_{c,\alpha\beta}}}\right)\right)^2 \tag{22}$$

$$b_\alpha = 0.077796 \frac{RT_{c,\alpha}}{p_{c,\alpha}} \tag{23}$$

$$c_{\alpha\beta} = 0.37464 + 1.54226\omega_{\alpha\beta} - 0.26992\omega_{\alpha\beta}^2 \tag{24}$$

where $T_{c,\alpha}$ and $p_{c,\alpha}$ are the critical temperature and pressure of species α, respectively. The critical mixture conditions for temperature $T_{c,\alpha\beta}$, pressure $p_{c,\alpha\beta}$ and acentric factor $\omega_{c,\alpha\beta}$ are determined using the corresponding state principles [16].

Partial derivatives and thermodynamic quantities based on the PR-EoS that are required for evaluating other thermodynamic variables can be derived analytically, as given below:

$$\left(\frac{\partial p}{\partial T}\right)_{v,X_i} = \frac{R}{v-b} - \frac{(\partial a/\partial T)_{X_i}}{v^2 + 2bv - b^2} \tag{25}$$

$$\left(\frac{\partial p}{\partial T}\right)_{T,X_i} = -\frac{RT}{(v-b)^2}\left\{1 - 2a\left[RT(v+b)\left(\frac{v^2+2bv-b^2}{v^2-b^2}\right)^2\right]^{-1}\right\} \tag{26}$$

$$\left(\frac{\partial a}{\partial T}\right)_{X_i} = -\frac{1}{T}\sum_{\alpha=1}^{N_s}\sum_{\beta=1}^{N_s} X_\alpha X_\beta a_{\alpha\beta} G_{\alpha\beta} \tag{27}$$

$$\left(\frac{\partial^2 a}{\partial T^2}\right)_{X_i} = 0.457236 \frac{R^2}{2T}\sum_{\alpha=1}^{N_s}\sum_{\beta=1}^{N_s} X_\alpha X_\beta c_{\alpha\beta}\left(1 + c_{\alpha\beta}\right)\frac{T_{c,\alpha\beta}}{p_{c,\alpha\beta}}\sqrt{\frac{T_{c,\alpha\beta}}{T}} \tag{28}$$

$$G_{\alpha\beta} = \frac{c_{\alpha\beta}\sqrt{T/T_{c,\alpha\beta}}}{1 + c_{\alpha\beta}\left(1 - \sqrt{T/T_{c,\alpha\beta}}\right)} \tag{29}$$

$$K_1 = \int_{+\infty}^{v} \frac{dv}{v^2 + 2bv - b^2} = \frac{1}{\sqrt{8b}} \ln\left(\frac{v + (1-\sqrt{2})/b}{v + (1+\sqrt{2})/b}\right) \tag{30}$$

For real fluids, thermodynamic quantities are typically evaluated from the ideal-gas value plus a departure function that accounts for the deviation from the ideal-gas behavior. The ideal-gas enthalpy, entropy and specific heat are evaluated from the NASA polynomials at a reference temperature of 298 K. The specific internal energy can be written as

$$e(T, \rho, X_i) = e^{ig}(T, X_i) + \int_0^{\rho}\left[p - T\left(\frac{\partial p}{\partial T}\right)_{\rho,X_i}\right]\frac{d\rho}{\rho^2} \tag{31}$$

where superscript "ig" indicates the ideal-gas value of the thermodynamic quantity, and Eq. (31) can be integrated analytically for PR-EoS to give

$$e = e^{ig} + K_1\left[a - T\left(\frac{\partial a}{\partial T}\right)_{X_i}\right] \tag{32}$$

where K_1 is evaluated using Eq. (30). The specific enthalpy can be expressed as:

$$h = h^{ig} - RT + K_1\left[a - T\left(\frac{\partial a}{\partial T}\right)_{X_i}\right] + pv \tag{33}$$

The specific heat capacity at constant volume and constant pressure, respectively, are evaluated as

$$c_v = \left(\frac{\partial e}{\partial T}\right)_{v,X_i} = c_v^{ig} - K_1 T\left(\frac{\partial^2 a}{\partial T^2}\right)_{X_i} \tag{34}$$

$$c_p = \left(\frac{\partial h}{\partial T}\right)_{p,X_i} = c_p^{ig} - R - K_1 T\left(\frac{\partial^2 a}{\partial T^2}\right)_{X_i} - T\frac{(\partial p/\partial T)_{v,X_i}^2}{(\partial p/\partial v)_{T,X_i}} \tag{35}$$

The speed of sound for a real fluid is given by

$$c^2 = \left(\frac{\partial p}{\partial \rho}\right)_{s,X_i} = \frac{\gamma}{\rho\kappa_T} \tag{36}$$

Downloaded by STANFORD UNIVERSITY on January 17, 2019 | http://arc.aiaa.org | DOI: 10.2514/6.2019-2143

where γ is the specific heat ratio and κ_T is the isothermal compressibility defined as

$$\kappa_T = -\frac{1}{v}\left(\frac{\partial v}{\partial p}\right)_{T,X_i} \tag{37}$$

The specific heat ratio is linearized around temperature to eliminate the costly iterative procedure to determine temperature, and also to obtain other thermodynamic quantities which are functions of temperature. The underlying strategy rests on correcting the tabulated values with the transported quantities based on the EoS used. Specifically, since PR-EoS is employed, along with thermodynamic quantities needed for evaluation of the ideal gas thermodynamic quantities, parameters *a* and *b*, and the first and second derivatives of the parameter *a* w.r.t. temperature are needed for the calculations of the partial derivatives in Eqs. (25)-(28) which are required for the evaluation of the departure functions. However, the parameter *a*, along with its derivatives, is a function of both the species composition and the temperature, and thus may not be consistent with the temperature corresponding to the transported variables. The following procedure is adopted for the evaluation of the parameter *a* and its derivatives: the dependence of the parameter *a* on temperature is assumed to be a quadratic function as follows:

$$a = C_1\tilde{T}^2 + C_2\tilde{T} + C_3 \tag{38}$$

where the coefficients C_1, C_2, C_3 can be obtained from tabulated quantities:

$$C_1 = \frac{1}{2}\left(\frac{\partial^2 a}{\partial T^2}\right)_0 \tag{39}$$

$$C_2 = \left(\frac{\partial a}{\partial T}\right)_0 - 2C_1T_0 \tag{40}$$

$$C_3 = a_0 - C_1T_0^2 - C_2T_0 \tag{41}$$

where subscript "0" indicates the stored baseline quantities in the table. The real-fluid energy is then evaluated as

$$\tilde{e} = \tilde{e}^{ig} + \tilde{e}^{dep} \tag{42}$$

where $\tilde{e}^{ig}$ and $\tilde{e}^{dep}$ are the ideal-gas and departure function values of the internal energy. The ideal-gas value including the chemical energy of the mixture is calculated with linearized specific heat ratio:

$$\tilde{e}^{ig} = \tilde{e}_0^{ig} + \frac{\tilde{R}}{a_\gamma^{ig}}\ln\left(1 + \frac{a_\gamma^{ig}(\tilde{T} - T_0)}{\tilde{\gamma}_0^{ig} - 1}\right) \tag{43}$$

where T_0, $\tilde{e}_0^{ig}$, $\tilde{R}$, a_γ^{ig}, $\tilde{\gamma}_0^{ig}$ are parametrized with $\tilde{Z}, \tilde{Z}''^2, \tilde{C}$ and stored in the flamelet table. The departure function is given by

$$\tilde{e}^{dep} = K_1\left[a - \tilde{T}\left(\frac{\partial a}{\partial T}\right)_{X_i}\right] \tag{44}$$

where Eqs. (38)-(41) are used to compute the parameters required for PR-EoS. Temperature and density are obtained by a bracketed secant iteration method from the computed pressure and energy, using Eqs. (19) and (32), respectively.

Transport quantities are evaluated based on the method due to Chung et al [17, 18]. A power-law is used to approximate the temperature dependency:

$$\frac{\tilde{\mu}}{\tilde{\mu}_0} = \left(\frac{\tilde{T}}{T_0}\right)^{a_\mu} \tag{45}$$

$$\frac{\lambda}{\tilde{\lambda}_0} = \left(\frac{\tilde{T}}{T_0}\right)^{a_\lambda} \tag{46}$$

The new compressible flamelet methodology discussed above is thermodynamically consistent in the entire flow path of a rocket engine (from oxidizer and fuel manifolds to the exit of the nozzle) and completely circumvents the need for ad hoc compressibility corrections of the FPV model in Loci-STREAM.

C. Thickened Flame Closure

The basic idea in using Thickened Flame Closure is to move all turbulence closure for the chemical source terms out of the flamelet tables, bringing it instead into the governing PDEs being solved by the CFD solver. The concepts

Downloaded by STANFORD UNIVERSITY on January 17, 2019 | http://arc.aiaa.org | DOI: 10.2514/6.2019-2143

underlying thickened flame closure evolved from the analytical investigation of the fundamental conservation equations governing laminar premixed flames as well as the DNS solution of such flames [19]. In general, when attempting to numerically simulate the propagation of a premixed flame on a grid of finite resolution, one must be able to resolve the flame in order to avoid numerical difficulties. Resolving the flame implies that the flame thickness must be captured over multiple cells in the grid. Generally, however, an actual flame is much thinner than the minimum cell size in the mesh. From basic analytical work [19] it was found that if the molecular diffusivities in the governing equations are multiplied by a flame thickening factor, *F*, and at the same time the reaction rates in the governing equations are divided by the same factor, an equivalent thickened flame will result. This flame will be *F* times thicker than the original flame (and able to be resolved on the mesh), but will have the same flame speed as the original flame. Subsequent research [20], however, found that the resulting thickened flame did not respond in the same manner as the original flame to eddies in the flow field. Typically a flame exposed to swirling eddies in the flow will stretch and fold (or wrinkle). As a result of this, the surface area of the flame front separating unburned fuel and oxidizer is increased, leading generally to an increased net reaction rate and thus an increased heat release per unit volume around the flame front. In order to counter the reduction in stretching and wrinkling of the thickened flame compared to the original flame, a so-called efficiency function, *E*, was introduced into the formulation which effectively enhances the reaction rate term in the governing equations. The resulting governing equations for mixture fraction and progress variable in the flamelet formulation, when using thickened flame closure, appear as follows, where multiplicative factors due to the closure model appear in the diffusion terms:

$$\frac{\partial \bar{\rho} Z}{\partial t} + \frac{\partial \bar{\rho} u_j Z}{\partial x_j} = \frac{\partial}{\partial x_j}\left[\left(\bar{\rho} D(EF) + \frac{\mu_t}{Sc_t}\right)\frac{\partial Z}{\partial x_j}\right] \tag{47}$$

$$\frac{\partial \bar{\rho} C}{\partial t} + \frac{\partial \bar{\rho} \tilde{u}_j C}{\partial x_j} = \frac{\partial}{\partial x_j}\left(\bar{\rho} D(EF)\frac{\partial C}{\partial x_j}\right) + \bar{\rho}\dot{\omega}_C\left(\frac{E}{F}\right) \tag{48}$$

In the original thickened flame closure model (Colin [20]), the flame thickening factor was specified as a constant value in the range $5<F<30$. The efficiency function, E, on the other hand was determined on a point-by-point basis in the flow using a rather complex procedure designed to quantify the local flame wrinkling due to resolved and unresolved (sub-grid) flow motions and its effective increase in the local heat release. Vreman et al [21] designed a new variation of the thickened flame closure approach which is substantially easier to implement and is more amenable to the use of a variety of turbulence models (RANS, DES, LES). Noting that the multiplicative factor *EF* which multiplies the molecular diffusivity in Eq.(48) could be tied to the underlying turbulence model (giving a spatially-varying thickening of the flame), this product is given by the following relation:

$$F^{1+\alpha} = EF = \frac{D + \mu_t/(\bar{\rho} Sc_t) + D_n}{D} \tag{49}$$

One can see that the product *EF* is essentially the ratio of the total diffusion to the molecular diffusion. This total diffusion strictly includes the original laminar diffusion (*D*), the turbulent diffusion arising from the use of a turbulence model (μ_t is the eddy viscosity resulting from the turbulence model and Sc_t is the turbulent Schmidt number) as well as the diffusion (D_n) arising from the numerical treatment of the convection term in the governing equations (this last term is commonly neglected). As a result of this definition of *EF*, in actuality, no modification of the existing diffusion terms in Loci-STREAM need be made as the existing turbulent diffusion coefficient is exactly the product *D*EF* (referring to the equations above). One needs simply to be able to compute the factor (*E*/*F*) which then multiplies the chemical source terms. To this end, Vreman et al[21] proposed a simple model which relates the efficiency function E to the flame thickening factor as

$$E = F^{\alpha}, \quad 0 < \alpha < 2/3 \tag{50}$$

where the theoretical limits of α were originally established by Colin [20]. Using this relation, the final expression for the factor (*E*/*F*) which multiplies the chemical source term in the governing equations of Loci-STREAM assumes the following form:

$$\frac{E}{F} = (F)^{\alpha-1} \tag{51}$$

In order to visualize the effective smoothing that is being applied to the chemical source term, Table 1 shows values of (*E*/*F*) for various viscosity ratios (total viscosity/laminar viscosity) for given values of α. The general trend is evident whereby increasing viscosity ratios results in more damping of the chemical source term, whereas increasing flame wrinkling efficiency results in less damping of the chemical source term. For RANS simulations, in which the flame may be many cells thick, local damping factors can range anywhere from $0.1 < (E/F) < 0.5$. For DES and LES simulations in which the viscosity ratios are much lower, damping factor will generally fall in the range $0.8 < (E/F) < 0.95$. Reversion to proper DNS behavior is satisfied in the sense that as the eddy viscosity approaches zero, resulting

Downloaded by STANFORD UNIVERSITY on January 17, 2019 | http://arc.aiaa.org | DOI: 10.2514/6.2019-2143

in a viscosity ratio of unity, the damping factor (E/F) also approaches unity, implying no modification of the laminar reaction source term values.

Table 2. Values of E for different values of viscosity ratio and α

Viscosity ratio	$E = F^0$	$E = F^{1/2}$	$E = F^{2/3}$
0.01	0.991	0.997	0.998
0.1	0.913	0.970	0.982
1	0.513	0.801	0.875
10	0.095	0.457	0.624
20	0.050	0.369	0.549
50	0.021	0.274	0.459
100	0.010	0.218	0.401

IV. Results

A. Single Element Shear Coaxial Injector

The first test case used to test the flamelet methodology described above is based on experiments conducted by Pal et al [22]. The experimental setup consists of a single element shear coaxial injector, a main cylindrical combustion chamber and two GOX/GH2 preburners which provide hot, oxidizer-rich and fuel-rich streams. A schematic of their experimental setup is shown in Figure 6. The main chamber wall is instrumented with coaxial heat flux gauges which provide both temperature and heat flux profiles. Details of the experimental conditions are provided by Pal et al [22].

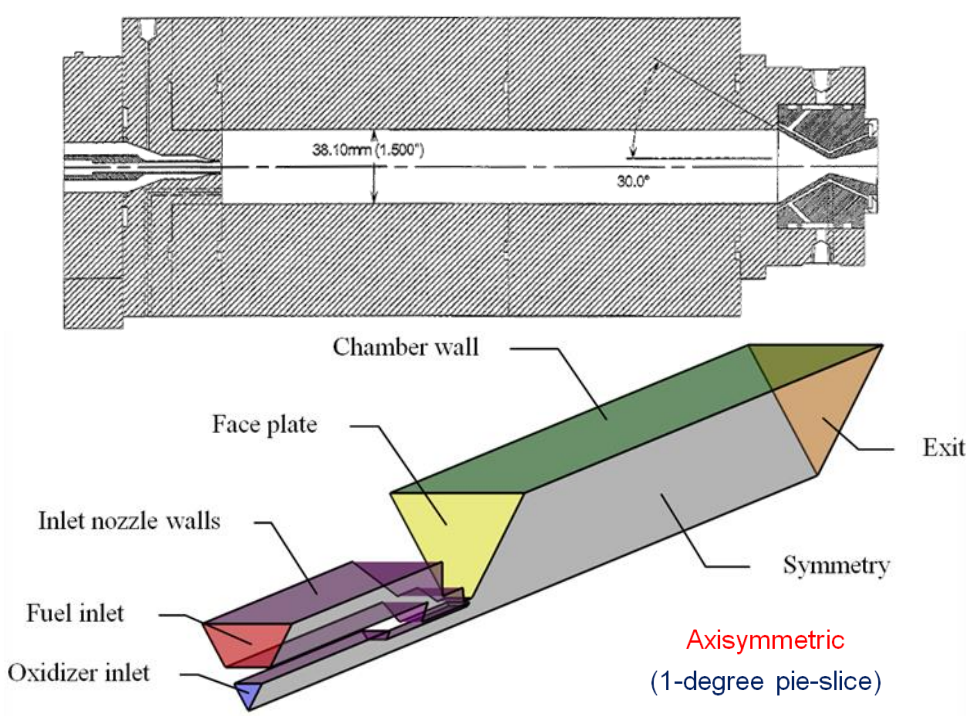

Figure 5. (Top) Schematic of the experiment[40] and (Bottom) schematic of the computational domain used for the simulations.

Downloaded by STANFORD UNIVERSITY on January 17, 2019 | http://arc.aiaa.org | DOI: 10.2514/6.2019-2143

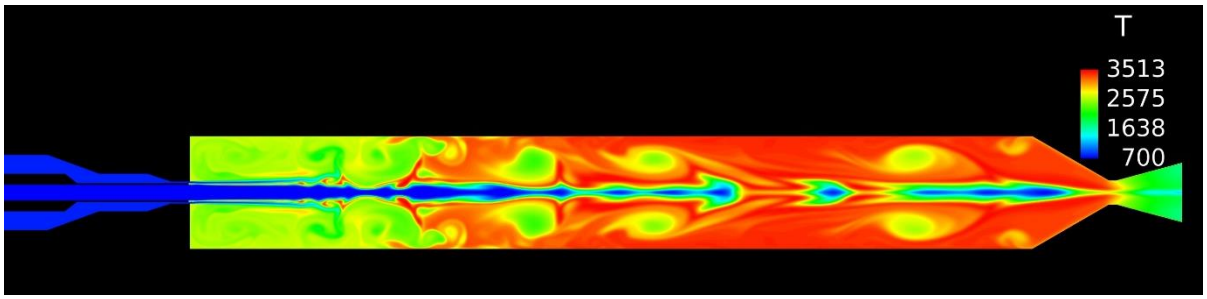

Figure 6. .Instantaneous temperature contour plot for the RCM1 injector (including the nozzle) the new compressible flamelet model in Loci-STREAM.

Downloaded by STANFORD UNIVERSITY on January 17, 2019 | http://arc.aiaa.org | DOI: 10.2514/6.2019-2143

Computational domain and boundary condition types for the injector geometry are shown in Figure 5. Axisymmetric domain is modeled with a 1-degree pie-shaped grid (circumferential dimension is exaggerated in Figure 6 for clarity). An extrapolated boundary condition is used at the supersonic exit, so the chamber pressure is not imposed but extrapolated from the solution. The simulation was conducted on a grid consisting of 175,000 cells. Figure 6 shows the temperature field for a DES simulation using a second-order upwind spatial scheme (SOU).

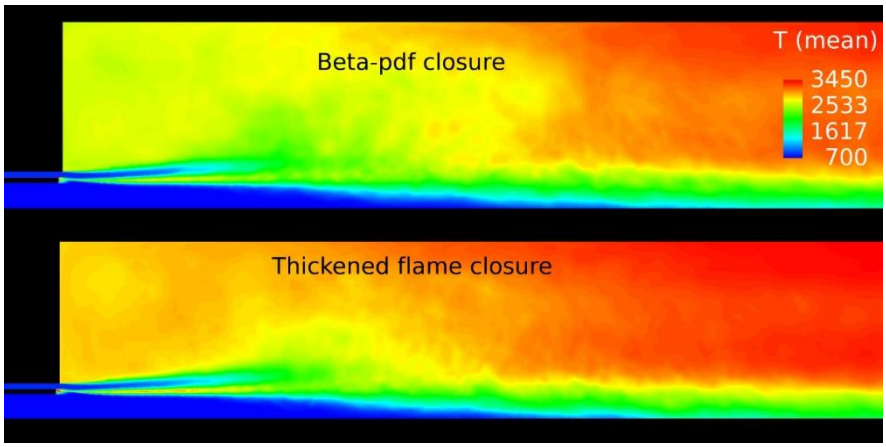

Figure 7. Mean (time-averaged) temperature contours for the RCM1 injector using beta-pdf and thickened flame closure models.

To test the new thickened-flame flamelet module in Loci-STREAM and to do a preliminary comparison of the differences between beta-pdf closure and thickened-flame closure, DES simulations of the adiabatic RCM-1 case were performed. A total of four cases were run, one with beta-pdf closure and three with thickened-flame closure ($E=F^0$, $E=F^{0.25}$ and $E=F^{0.5}$). For each case, a steady-state RANS simulation was first run for 5000 time steps with a time step of $dt=1x10^{-5}$. Next a DES simulation for each was run for an additional 20000 time steps with $dt=2x10^{-6}$ to fully-establish the unsteady flow. Finally each case was run for an additional 5000 time steps with $dt=2x10^{-6}$ to collect time-averaged data for the mean temperature. Figure 7 shows mean temperature contours for the beta-pdf closure case and the $E=F^{0.5}$ thickened-flame closure case. From these plots it is apparent that thickened-flame closure results in higher temperatures in the upper left recirculation zone compared to beta closure. Figure 8 shows mean temperature plotted along the upper wall for all four cases. All thickened-flame cases display higher temperatures in the recirculation zone. In addition, the expected result is obtained whereby increase flame wrinkling efficiency results in higher temperature in the recirculation zone for the thickened-flame cases. The maximum deviation at any wall location between the beta closure and $E=F^{0.5}$ thickened-flame closure case (which differs most from the beta closure case) is approximately 10%.

B. Tribrachial (Triple) Flame

As the second test case, a steady-state flame with known combustion characteristics, called the tribrachial flame, is simulated using the compressible flamelet solver in Loci-STREAM. A pictorial diagram of this flame is shown in Fig. 9, which can occur in a non-premixed rocket injector when the flame is not anchored at the post but instead there is flame lift-off. A triple flame contains different combustion regimes and represents a challenging test case for any single-regime combustion model as far as accuracy is concerned. Generally, tribrachial flames are present in flows

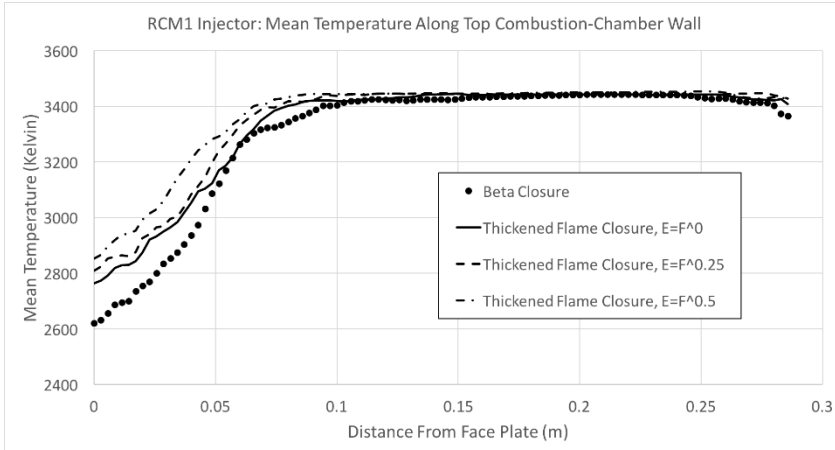

Figure 8. Mean temperature profiles along the upper wall of the RCM1 injector with thickened flame closure (different values of E/F) and beta-pdf closure.

with a stratification of reactants and represent multi- and mixed-regime rocket- combustion regimes, associated with flame blow-out, flame lift-off and combustion dynamics. A tribrachial (triple) flame consists of lean and rich premixed flame branches, and a diffusion flame embedded in between the two premixed branches. Within the diffusion flame, excess fuel from the rich premixed flame branch reacts with the excess oxidizer from the lean premixed flame branch. The three flame branches meet at the triple point at nearly stoichiometric composition. Furthermore, the mixture in the diffusion branch is usually close to chemical equilibrium and the diffusion flame is less prominent than the two premixed flames. Apart from the different flame regimes, tribrachial flames exhibit complex combustion-physical processes that are complicated by curvature, stretch rate, and preferential diffusion processes, therefore affecting the mass-burning rates in the premixed flame branches, radical production, and variations of the propagation speed. No single model (such as the FPV model in Loci- STREAM) will accurately model such a flame configuration – though it might yield a robust numerical solution! The only homogeneous model that would be accurate is Direct Numerical Simulation (DNS) but that is obviously out of the question for practical applications. By utilizing reaction-diffusion manifold models in regions where they are accurate for a user-defined threshold, simulations with the PEC approach are able to reproduce results comparable to the detailed chemistry simulation; however, at significantly reduced computational cost.

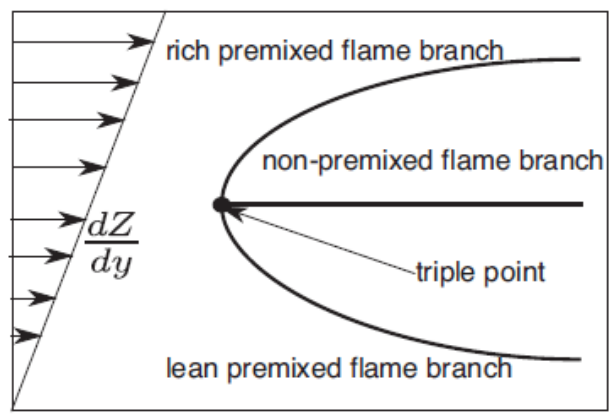

Figure 9 Schematic of the flame structure for a tribrachial flame.

Simulations have been performed with the Loci-STREAM compressible flamelet solver for the tribrachial flame. Table 3 below presents the key features of the simulations:

Table 3. Key features of the tribrachial flame simulations using Loci-STREAM	
Grids Used	201x151, 401x301
Reaction Mechanisms	DRM-19, GRI-3.0
Flamelets	FPV, 101x101 resolution table

Downloaded by STANFORD UNIVERSITY on January 17, 2019 | http://arc.aiaa.org | DOI: 10.2514/6.2019-2143

The tribrachial flame case is a good verification case partly because it verifies the ability of a solver to predict the proper flame speed. In general, the burning velocity of a tribrachial flame configuration is different than that of a uniform composition premixed flame, either lower or higher, depending on the mixture fraction stratification (transverse gradient in this case). Since the flame speed is not known a priori, in order to stabilize the tribrachial flame in the domain, one must use some form of control that adjusts the inlet velocity as time evolves until a steady-state flame is achieved that is fixed at a defined position in the domain. The final value of the velocity at the inlet of the domain is then the flame speed that is predicted by the solver. In order to accomplish this, a PID controller capability was added to Loci-STREAM in the form of a module specifically designed for the tribrachial flame case. The controller works by looking for the minimum streamwise location of any cell in the domain that contains a water mass fraction greater than a specified low cut-off (0.1 has been found to be a good value). Due to the physical characteristic of the tribrachial flame, this minimum streamwise location corresponds to the triple point (the conjunction of the lean premixed, rich premixed and weak central diffusion flame). The goal of the controller is to ensure that the triple point remains fixed at a prescribed location in the domain (x=0.25*L in this case, where L is the streamwise length of the domain, and centered in the transverse y direction). The equation that governs the PID controller is as follows:

$$-dv(t) \;=\; K_p e(t) \;+\; K_i \int_0^t e(t')\,dt' \;+\; K_d \frac{de(t)}{dt} \tag{52}$$

In this equation, the term dv represents the time-dependent velocity increment that is added to the current inlet velocity and e(t) represents the current deviation of the triple point from the desired set-point location (0.25*L). Thus, a positive deviation from the set-point location (i.e., when the flame moves too far downstream) results in a negative velocity increment added to the inlet velocity. Similarly a negative deviation from the set-point location results in a positive velocity increment. For the results to be presented, controller constants K_p =3.0, K_i =0.2 and K_d =0.0 were found to be suitable in providing a reliable stabilization of the flame.

(i) <u>DRM-10 Mechanism</u>

The DRM-19 mechanism consists of 21 species involved in 84 reactions. A 101x101 FPV flamelet table was created using a combination of FlameMaster to construct the counter-diffusion flamelets and the Loci-STREAM Flamelet Table Tool to generate the flamelet table from these flamelets. Simulations were performed on the 201x151 and 401x301 meshes. Figure 10 below shows a plot of the inlet velocity evolution with time. From the plot, we can see that the final Loci-STREAM flame speed, U=0.42 m/s, which is essentially independent of grid resolution. The

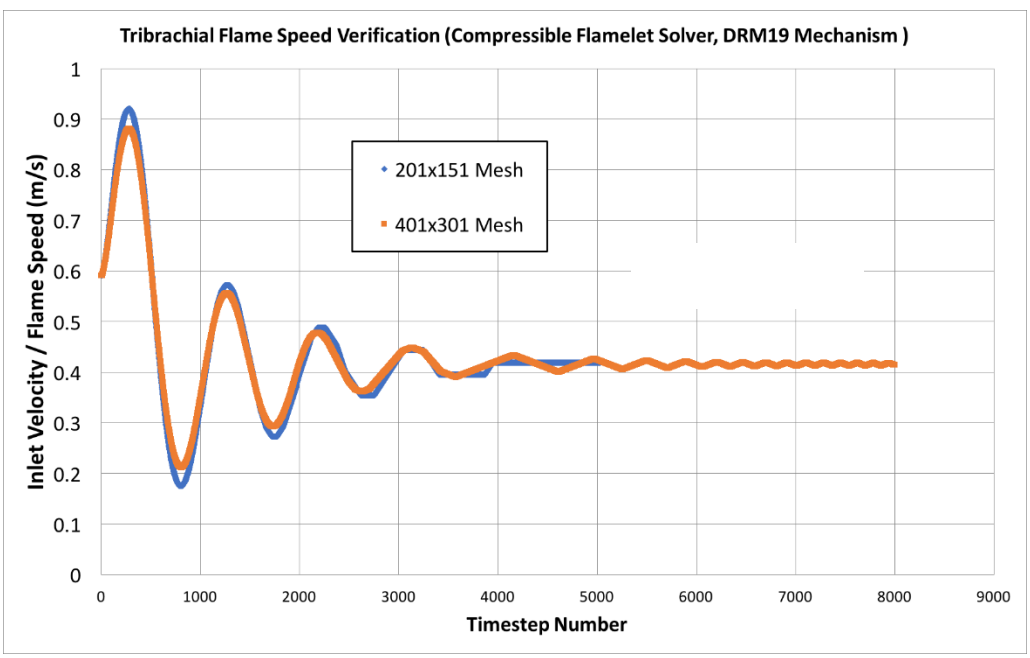

Figure 10. Evolution of inlet velocity with time using the DRM-19 mechanism using two meshes.

Downloaded by STANFORD UNIVERSITY on January 17, 2019 | http://arc.aiaa.org | DOI: 10.2514/6.2019-2143

Downloaded by STANFORD UNIVERSITY on January 17, 2019 | http://arc.aiaa.org | DOI: 10.2514/6.2019-2143

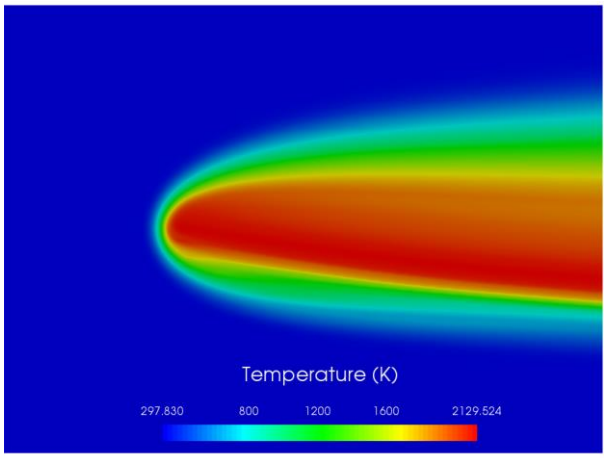

(a) Temperature

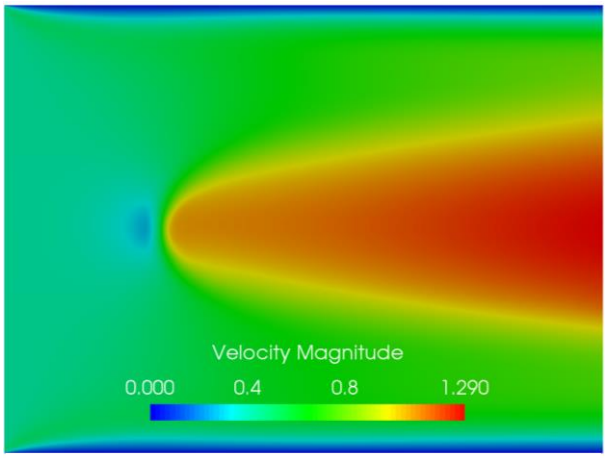

(b) Velocity magnitude

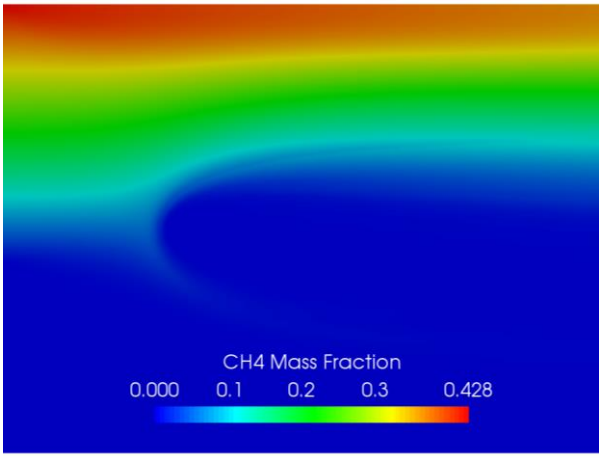

(c) CH4 mass fraction

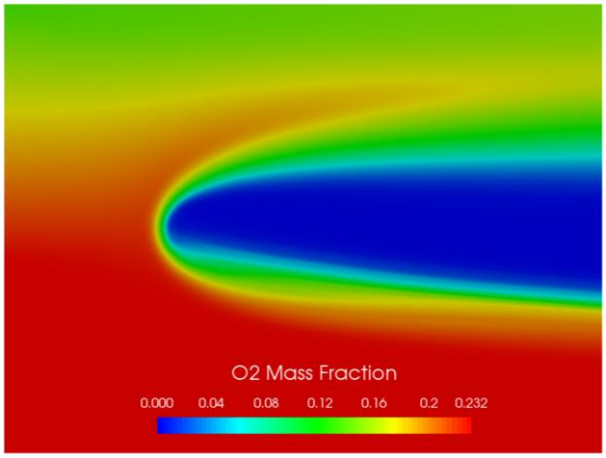

(d) O2 mass fraction

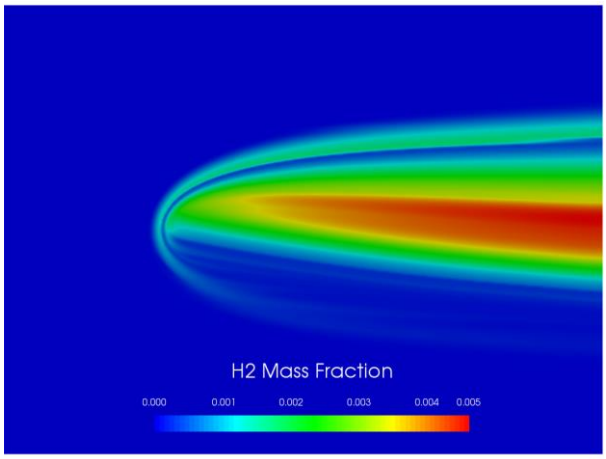

(e) H2 mass fraction

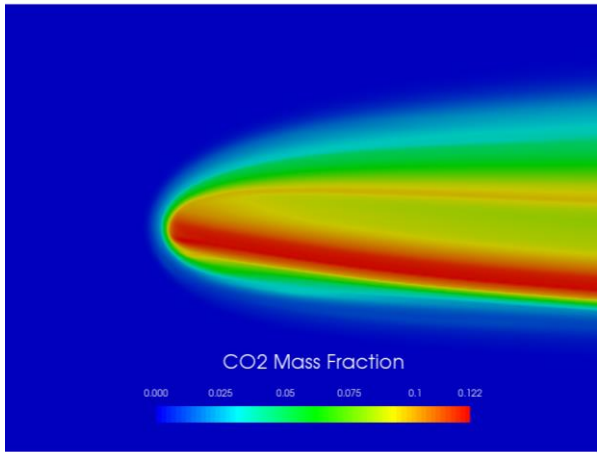

(f) CO2 mass fraction

Figure 11. Contours of temperature and certain primary species mass fractions for the tribrachial flame using the DRM-19 mechanism.

maximum flame temperature is 2129 K. The Loci-STREAM simulation captures the generation of the intermediate

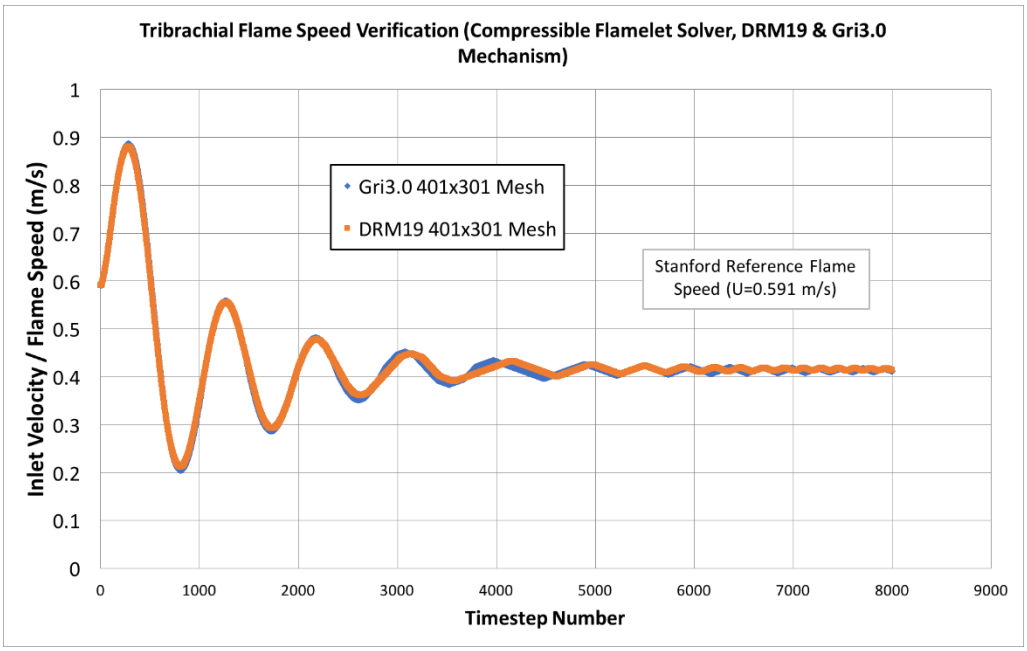

Figure 12. Evolution of inlet velocity with time using the DRM-19 and GRI-3.0 mechanisms on the 401x301 mesh.

fuels CO and H2 on the rich side (top side) of the flame which serve as the fuels for the diffusion flame at the center of the tribrachial flame (shown in Figure 11). The maximum CO mass fraction is 0.065. Other indicators of qualitative correctness of the Loci-STREAM results include the location, tilt (away from the rich side of the flame) and maximum value of the CO2 mass fraction, as well as the location of the maximum HCO mass fraction, which correlates well will the location of maximum heat release (not shown in the figure).

(ii) <u>GRI-3.0 Mechanism</u>

The GRI-3.0 mechanism consists of 53 species involved in 325 reactions. Similarly to the DRM-19 case above, a 101x101 flamelet table was generated. Simulations were performed on the 401x301 mesh. Figure 12 shows a plot of the inlet velocity evolution with time compared with the DRM-19 401x301 mesh simulation. The steady-state flame speed value is nearly identical to the value obtained using the DRM-19 mechanism. Contours of the temperature field and primary species mass fractions are qualitatively similar to the DRM-19 result, but vary quantitatively due to the increased mechanism fidelity.

V. Summary

A robust unsteady turbulent compressible combustion modeling capability developed in a CFD solver called Loci-STREAM is presented in this paper. It utilizes the flamelet methodology extended to account for compressibility involving both ideal and real fluids. The ideal-gas thermodynamics is modeled by linearizing the specific heat ratio whereas the parameters needed for the cubic Peng Robinson equation of state are pre-tabulated for the evaluation of departure functions and a quadratic expression is used to model the attraction parameter. This compressible model is able to account for temperature and pressure variations from the baseline flamelet table. A laminar triple flame configuration and a single element shear coaxial rocket injector are used as test cases to validate this compressible flamelet solver.

Downloaded by STANFORD UNIVERSITY on January 17, 2019 | http://arc.aiaa.org | DOI: 10.2514/6.2019-2143

References

[1] Thakur, S., Wright, J. and Ihme, M., "Parallel Compressible Solver for Unsteady Turbulent Combustion in Rocket Injectors Using Flamelet Models," 21st AIAA Computational Fluid Dynamics Conference, San Diego, June 24-27 2013, AIAA-2013-2835 (2013).

[2] Ma, P.C., Banuti, D.T. and Ihme, M., "Numerical framework for transcritical real-fluid reacting flow simulations using the flamelet progress variable approach," AIAA-2017-0143 (2017).

[3] Thakur, S. and Wright, K., "An All-Speed Solver for Unsteady Reacting and Non-Reacting Flows Using a Rule-Based Framework," 42nd AIAA Fluid Dynamics Conference, #AIAA-2012-3254 (2012).

[4] Luke, E.A., "LOCI: A Deductive Framework for Graph-Based Algorithms," *Third International Symposium on Computing in Object-Oriented Parallel Environments*, edited by S. Matsuoka, R. Oldehoeft and M. Tholburn, No. 1732 in Lecture Notes in Computer Science, Springer-Verlag, pp 142-153 (Dec. 1999).

[5] Peters, N., "Turbulent Combustion," Cambridge University Press (2000).

[6] Ihme, M., Cha, C.M. and Pitsch, H., "Prediction of local extinction and re-ignition effects in nonpremixed turbulent combustion using a flamelet/progress variable approach," Proc. Combust. Inst., 30:793–800 (2005).

[7] Pierce, C. D. and Moin, P. "Progress-variable approach for large-eddy simulation of non-premixed turbulent combustion." J. Fluid Mech. 504, 73-97, (2004).

[8] Thakur, S., Wright, J., Ihme, M. and Tucker, P.K., "Simulation of a Shear Coaxial GO2/GH2 Rocket Injector with DES and LES Using Flamelet Models," 48th AIAA/ASME/SAE/ASEE Joint Propulsion Conference, #AIAA-2012-3744 (2012).

[9] Patankar, S. V., Numerical Heat Transfer and Fluid Flow, Hemisphere, Washington, DC (1980).

[10] Rhie, C.L. and Chow, W.L., "A Numerical Study of the Turbulent Flow Past an Isolated Airfoil with Trailing Edge Separation," *AIAA Journal*, **21**: 1525-1532 (1983).

[11] Strelets, M. 2001, "Detached Eddy Simulation of Massively Separated Flows," *AIAA Paper 2001-0879*.

[12] Peng, D.-Y. and Robinson, D. B., "A new two-constant equation of state," Ind. Eng. Chem. Res., Vol. 15, No. 1, pp. 59-64 (1976).

[13] Ely, J. F. and Hanley, H., "Prediction of transport properties. 1. Viscosity of fluids and mixtures," Ind. Eng. Chem. Res., Vol. 20, No. 4, pp. 323-332 (1981).

[14] Ely, J. F. and Hanley, H., "Prediction of transport properties. 2. Thermal conductivity of pure fluids and mixtures," Ind. Eng. Chem. Res., Vol. 22, No. 1, pp. 90-97 (1983).

[15] Harstad, K. G., Miller, R. S., and Bellan, J., "Efficient high-pressure state equations," AIChE J., Vol. 43, No. 6, pp. 1605-1610 (1997).

[16] Poling, B.E., Prausnitz, J.M., and O'Connell, J.P., The properties of gases and liquids, McGraw-Hill New York, (2001).

[17] Chung, T.H., Lee, L.L., and Starling, K.E., "Applications of kinetic gas theories and multiparameter correlation for prediction of dilute gas viscosity and thermal conductivity," Ind. Eng. Chem. Res., Vol. 23, No. 1, pp. 8-13 (1984).

[18] Chung, T. H., Ajlan, M., Lee, L. L., and Starling, K. E., "Generalized multiparameter correlation for nonpolar and polar fluid transport properties," Ind. Eng. Chem. Res., Vol. 27, No. 4, pp. 671-679 (1988).

[19] Legier, JP, Poinsot, T and Veynante, D, "Dynamically thickened flame LES model for premixed and non-premixed turbulent combustion," Center for Turbulence Research Proceedings of the Summer Program, p 157-168 (2000).

[20] Colin, O., Ducros, F, Veynante, D and Poinsot, T, "A thickened flame model for large eddy simulations of turbulent premixed combustion," Physics of Fluids 12, pp 1843-1863 (2000).

[21] Vreman, AW, Albrecht, BA, van Oijen, J.A, de Goey, LPH, Bastiaans, RJM, "Premixed and nonpremixed generated manifolds in large-eddy simulation of Sandia flame D and F," Combustion and Flame 153, pp 394–416 (2008).

[22] Pal, S., Marshall, W., Woodward, R. and Santoro, R., "Wall heat flux measurements for a uni-element GO2/GH2 shear coaxial injector," Third International Workshop on Rocket Com-bustion Modeling, Paris, France, March, 13-15 (2006).

Downloaded by STANFORD UNIVERSITY on January 17, 2019 | http://arc.aiaa.org | DOI: 10.2514/6.2019-2143